ACCOUNTS of chemical research

Article

pubs.acs.org/accounts

Structural Investigations of Self-Assembled Monolayers for Organic Electronics: Results from X-ray Reflectivity

Artoem Khassanov,[†] Hans-Georg Steinrück,[‡] Thomas Schmaltz,[†] Andreas Magerl,[§] and Marcus Halik*[,†]

[†]Organic Materials & Devices (OMD), Friedrich-Alexander-Universität Erlangen-Nürnberg, Martensstrasse 7, 91058 Erlangen, Germany

[‡]Crystallography and Structural Physics, Friedrich-Alexander-Universität Erlangen-Nürnberg, Staudtstrasse 3, 91058 Erlangen, Germany

[§]Physics Department, Friedrich-Alexander-Universität Erlangen-Nürnberg, Staudtstrasse 3, 91058 Erlangen, Germany

Supporting Information

CONSPECTUS: Self-assembled monolayers (SAMs) have been established as crucial interlayers and electronically active layers in organic electronic devices, such as organic light emitting diodes (OLEDs), organic photovoltaics (OPVs), organic thin film transistors (OTFTs), and nonvolatile memories (NVMs). The use of self-assembling functionalized organic molecules is beneficial due to mainly three advantages compared with common thin film deposition approaches. (1) Molecular self-assembly occurs with surface selectivity, determined by the interaction between the functional anchor group of the organic molecules and the target surface. (2) The film thickness of the resulting layers is perfectly controllable on the angstrom scale, due to the self-terminating film formation to only a single molecular layer. And finally, (3) the wide variability in the chemical structure of such molecules enables different SAM functionalities for devices, ranging from electrical insulation to charge storage to charge transport. The SAM approach can be further expanded by employing several functionalized molecules to create mixed SAMs with consequently mixed properties.

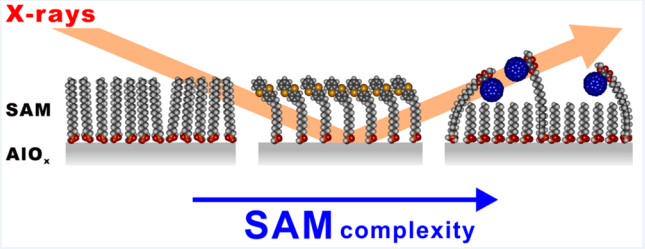

The function of SAMs in devices depends not only on the chemical structure of the molecules but also on their final arrangement and orientation on the surface. A reliable and nondestructive in-depth characterization of SAMs on nonconductive oxide surfaces is still challenging because of the very small thickness and the impracticality of methods such as scanning tunneling microscopy (STM) and X-ray photoelectron spectroscopy (XPS).

In this Account, we illustrate how X-ray reflectivity (XRR) provides analytical access to major questions of SAM composition, morphology, and even formation by means of investigations of pure and mixed SAMs based on phosphonic acids (PAs) of various chain structures on flat alumina (AlO_x) surfaces. XRR is an analytical method that provides access to spatially averaged structural depth profiles over a relatively large area of several square micrometers. The key outcome of XRR, the surface-normal electron density profile of the SAMs, leads to precise information on the SAM thickness with subangstrom resolution and allows for the determination of molecular tilt angles and packing densities.

We have systematically increased the chemical complexity of PA molecules and the resulting SAMs, utilizing XRR to provide insight into the SAM structures. In SAMs composed of functionalized molecules or complex chain structures, the distribution of electron rich and electron poor signatures is detected and thus the molecular order within the SAM is determined.

In mixed SAMs of two different molecular species, electron density profiles reveal the morphology and how the surface-normal structure changes if one component of the mixed SAM is altered. Furthermore, XRR was applied to investigate in situ the self-assembly of functionalized PA molecules from solution by tracking the monolayer growth over time. Even though the results provided by XRR on in-plane molecular arrangement are limited, it presents excellent information on the molecular scale along the surface normal and in addition allows for drawing conclusions on the intermolecular interactions within the SAM.

1. INTRODUCTION

The use of self-assembled monolayers (SAMs) for surface modification is a well-established tool, besides their application in organic electronics.[1−3] For almost any surface, complementary molecular structures have been developed to create densely packed monolayers by self-assembly. The approach has been extended far beyond the most prominent examples of thiols[4,5] on gold and silver or silanes[6] on oxide surfaces. In most cases, long and linear molecular structures, anchored on the surface by reactive groups, are utilized. These SAMs are typically illustrated as densely packed, upright-standing molecules with an optional tilt and a well-ordered arrangement. However, for accurate statements on the structure of the SAMs,

Received: January 16, 2015
Published: June 15, 2015

DOI: 10.1021/acs.accounts.5b00022
Acc. Chem. Res. 2015, 48, 1901−1908

analytical methods are required to provide results on packing density and molecular orientation, in particular for functional molecules of complex shape.[7] Conventional techniques such as static contact angle measurements, ellipsometry, or infrared spectroscopy alone are insufficient to answer all general questions regarding the structure of the SAMs. In order to elaborate these, several experimental methods are used. Near edge X-ray absorption fine structure spectroscopy (NEXAFS),[8] infrared reflection−adsorption spectroscopy (IRRAS),[9] Fourier transform infrared spectroscopy (FTIR),[10] sum frequency generation (SFG),[11] and grazing incidence X-ray diffraction (GIXD)[12] are typically applied to investigate the molecular orientation. A complementary method is X-ray reflectivity (XRR), which is a nondestructive, spatially averaging technique for the investigation of thin films. The thickness, density, and roughness of individual sublayers can be resolved independently. This allows, together with preknowledge such as the chemical composition of the molecules, for an in-depth understanding of structural properties of simple and complex SAMs, as we show below.

2. METHODS

2.1. Self-Assembly of Phosphonic Acid Based Molecules

SAMs made of phosphonic acids ($R\text{-}PO(OH)_2$) have been thoroughly utilized in combination with metal oxide surfaces, such as alumina (AlO_x),[13] titania (TiO_x),[14] and indium tin oxide (ITO).[1] Most research groups applied simple solution based processing techniques by immersing the substrate in a solution of phosphonic acids (PAs). Typically, the strong binding of PAs leads to a fast self-assembly[15] and even enables transfer printing techniques.[16] Solutions within concentrations between 0.005 and 0.1 mM in 2-propanol (IPA) are favorable for reasonable processing times.

The self-assembly of alkyl-PAs is self-terminating and restricted by the availability of anchoring sites and space on the metal oxide surface.[4] The formation of multilayers is prevented, and the monolayer thickness is determined by the length of the molecules and their arrangement on the surface (tilt, entanglement, etc.). Even though the true binding mechanism of PAs on metal oxides is still not fully resolved,[6] it is unquestionable that self-assembly leads to reproducible, high-quality monolayers in a simple and robust process. The molecular design of PA molecules follows the universal blueprint of almost all SAM molecules, with a surface selective anchor group, a long alkyl chain, and a headgroup (Figure 1a). The length of the molecule and, more strongly, the functionalization of the headgroup determine the final properties of the monolayer.

A simple example for applications of SAMs based on PAs in organic electronics is the use of *n*-alkyl PAs (Figure 1a) as part of a thin dielectric layer[17] of an OTFT. Due to the high capacitance of the dielectric stack (SAM/thin AlO_x), the devices operate at low supply voltages of about 3 V or less. The gate dielectric approach was extended to phosphonic acid molecules with functionalization (e.g., fluorinated phosphonic acids, Figure 1a), which not only provide low-voltage operation but also impact the threshold voltage (V_{th}) in devices.[18] To fine-tune these changes in properties, it is possible to utilize mixed SAMs.[19] These are used for the fabrication of memory OTFTs,[20] with integrated charge storage SAMs consisting of fullerene functionalized PA and insulating alkyl-PA molecules, and active charge-transport layers in self-assembled monolayer field-effect transistors (SAMFETs).[21,22] Another method to modify SAMs and to obtain specific properties is the use of exchange reactions.[15,23]

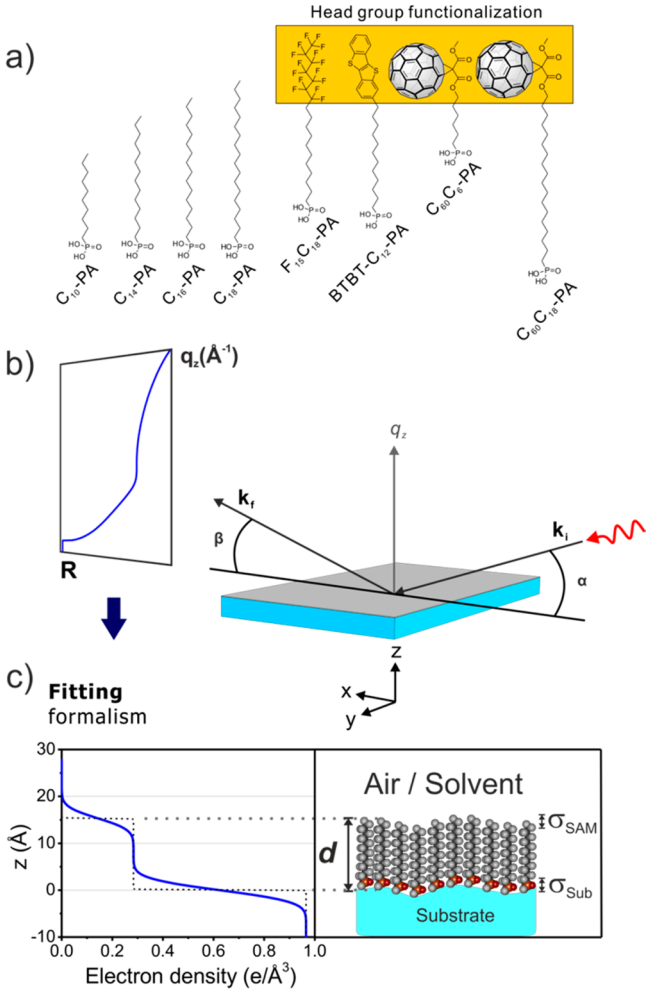

Figure 1. (a) Chemical structures of phosphonic acid (PA) molecules investigated in this Account. The headgroup functionalization is depicted in the yellow box. (b) Reflectivity setup with impinging X-rays at an incoming angle α, which are being detected at the outgoing angle β (= α). (c) Exemplary electron density profile of a SAM on a solid substrate, together with its interpretation with SAM thickness (d), and SAM (σ_{SAM}) and substrate roughness (σ_{Sub}).

2.2. X-ray Reflectivity

XRR measures the intensity fraction of an incoming X-ray beam that is specularly reflected from a sample. Figure 1b illustrates the kinematics of this process. The incident X-ray impinges on the surface under an angle α in the (x,y)-plane. Specular reflection is observed within the plane of incidence at an exit angle β equal to the incoming angle α. In this setup, the wave vector transfer has a component solely perpendicular to the surface (z-direction), with $q_z = \mathbf{k}_f - \mathbf{k}_i = 4\pi/\lambda \sin \alpha$, where $\mathbf{k}$ is the wave vector, $|\mathbf{k}| = k = 2\pi/\lambda$ is the wavenumber, and λ the X-ray wavelength.[24]

For X-rays, the index of refraction can be written as $n = 1 - \delta - i\beta$.[24] Here, $\delta = \lambda^2 r_e \rho_e/(2\pi)$ is the dispersion term, where r_e is the classical electron radius, ρ_e is the electron density, and $\beta = \lambda\mu_0/(4\pi)$ is the absorption term, where μ_0 is the linear absorption coefficient. Since δ and β are positive, the refraction index is slightly smaller than unity, implying that X-rays are

DOI: 10.1021/acs.accounts.5b00022
Acc. Chem. Res. 2015, 48, 1901−1908

totally externally reflected below a critical angle α_c, when traveling into a denser medium.

The simplest example for the reflection of X-rays is an ideally sharp interface between two media of different electron densities. The reflected signal, for simplicity from a vapor−media interface and neglecting absorption, can be derived by matching the wave fields at this interface, which yields the so-called Fresnel reflectivity.[24]

$$R_F(q_z) = \left| \frac{q_z - \sqrt{q_z^2 - q_c^2}}{q_z + \sqrt{q_z^2 - q_c^2}} \right|^2$$

For a flat sample, a variation in the electron density profile along the surface normal with a length scale of d results in characteristic oscillatory reflection features in reciprocal space with a period of $\Delta q_z = 2\pi/d$. These so-called Kiessig fringes appear due to constructive and destructive interferences of waves reflected at the individual interfaces.

An arbitrary density profile is modeled by slicing it into thin slabs of constant electron density. The reflectivity is then calculated recursively via the dynamical theory of reflections (for a detailed explanation see ref 24 and references therein). Here, the wave fields at each interface have to be matched, yielding the corresponding Fresnel reflection and transmission coefficients. Smearing of these interfaces, due to interfacial roughness in real systems, is described by a Debye−Waller-like factor of the form $e^{-q_z^2\sigma_j^2/2}$, where σ_j represents a Gaussian roughness of the jth slab.[24] In practice, an electron density profile, $\rho_e(z)$ (Figure 1c), is built up by a certain number of physically meaningful slabs, using preknowledge, such as chemical composition of molecules within the SAM. Each slab has a uniform, but variable, electron density, thickness, and roughness. The calculated reflectivity is then compared with the experimental data. In an iterative process, the parameters of the slabs are varied until the calculated and experimental curves match.[25] Details of the XRR analysis specific to our systems as well as details of parameter confidence intervals and correlations are presented in the Supporting Information.

The XRR measurements presented in this Account were carried out at (1) beamline ID10[26] at the European Synchrotron Radiation Facility in Grenoble using 22.0 keV X-rays and (2) a Bruker D8 reflectometer using 17.5 keV X-rays.

3. CHARACTERIZATION OF PRISTINE SAMs WITH XRR

3.1. *N*-Alkyl Phosphonic Acid SAMs

The most general analytical issues in SAM applications are the orientation of the molecules and the quality of a SAM on a surface. This qualitative information can be translated into the quantitative values of SAM thickness, allowing for an estimation of the molecular tilt angle, and the packing density of the molecules. XRR enables access to these parameters, as shown for the investigation of a series of *n*-alkane PAs (Figure 2).

The surface-normal structure of three *n*-alkyl PAs (decylphosphonic acid, C_{10}-PA; tetradecylphosphonic acid, C_{14}-PA; octadecylphosphonic acid, C_{18}-PA) self-assembled on atomic layer deposition grown (ALD) AlO_x is identified by modeling the XRR curves and extracting the laterally averaged surface-normal electron density profiles. Figure 2a shows the Fresnel-normalized reflectivity (R/R_F) curves, together with the corresponding model fits. The fit-derived electron density profile is depicted in Figure 2b and the best fit parameters are

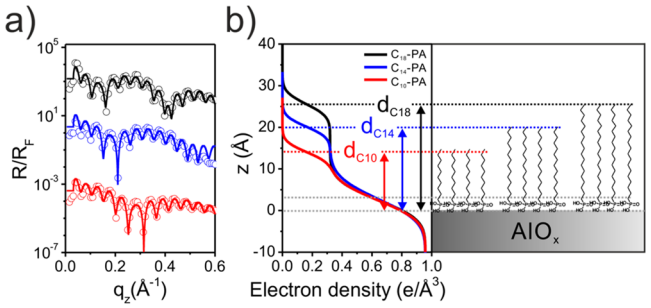

Figure 2. (a) Measured R/R_F (circles) of a C_{10}-PA (red), C_{14}-PA (blue), and C_{18}-PA (black) SAM on AlO_x, with corresponding fits (solid lines). Curves are shifted for clarity. (b) Fit-derived electron density profiles and schematic interpretation of the self-assembled *n*-alkyl PAs with a nearly perpendicular arrangement relative to the surface.

tabulated in the Supporting Information. The short period oscillations, as observed in all XRRs in this Account, correspond to the Kiessig fringes yielding from the ALD grown AlO_x layer with a thickness of approximately 120 Å. The electron density profile used in the fits is constructed with three slabs, namely, the AlO_x, the surface-adjacent PA anchor group (for details, see Supporting Information), and the hydrocarbon chain.

This analysis shows a self-terminating monolayer assembly and excludes double- or multilayer formation. The film thickness d of the SAM was determined as 14.3 Å for C_{10}-PA, 20.1 Å for C_{14}-PA, and 25.8 Å for C_{18}-PA (Figure 2b). These values are in excellent agreement with theoretical values of the molecular length for C_{10}-PA of approximately 15.7 Å, for C_{14}-PA of 20.8 Å, and for C_{18}-PA of 25.9 Å, suggesting an almost perpendicular orientation of these *n*-alkyl PAs with respect to the surface. The electron density of the three alkyl SAMs of 0.32 e/Å^3 is in the range of typical values for hydrocarbon chains in the rotator phase.[27] With this information, that is, electron density and thickness of the monolayer d, we have calculated the space requirement A per alkyl-PA molecule[28] as 22.5 Å^2 per C_{10}-PA, 20.7 Å^2 per C_{14}-PA and 19.9 Å^2 per C_{18}-PA molecule. Notably, as previously reported,[29] a denser packing is obtained for longer alkyl chains, indicating that shorter alkyl chains tend to organize into amorphous films whereas longer ones exhibit crystalline domains.

3.2. Functionalized *N*-Alkyl PA SAMs

XRR offers the possibility to compare the surface-normal electron density distribution between functionalized and simple, nonfunctionalized SAMs (e.g., C_n-PA) to draw precise conclusions on the morphology of the molecular components. A monolayer of 12,12,13,13,14,14,15,15,16,16,17,17,18,18,18*H*-pentadecafluoro-octadecyl phosphonic acid ($F_{15}C_{18}$-PA, Figure 1a) with 15 fluorine atoms (C_{18}-PA with partially substituted hydrogen atoms) was investigated. The molecule has a similar theoretical length as C_{18}-PA but with a presumably higher electron density due to the electron rich fluorine. The measured R/R_F and its fit, assuming a four-slab model (AlO_x, PA anchor group, alkyl chain, fluorine functionalized alkyl), are shown in Figure 3a. The corresponding electron density profile (Figure 3b, best fit values in Supporting Information, Table 1) shows a characteristic minimum in ρ_e of 0.27 e/Å^3 attributed to the nonfluorinated alkyl chain, between two electron rich sections (AlO_x and fluorinated alkyl chain). The length of the electron-

DOI: 10.1021/acs.accounts.5b00022
Acc. Chem. Res. 2015, 48, 1901−1908

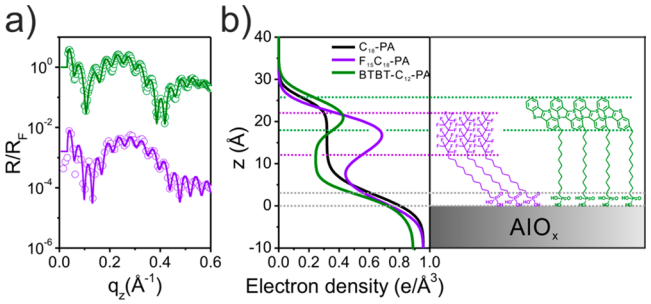

Figure 3. (a) Measured R/R_F (circles) of a $F_{15}C_{18}$-PA (purple) and BTBT−C_{12}-PA[34] (green) SAM on AlO_x, with corresponding fits (solid lines). Curves are shifted for clarity. (b) Fit-derived electron density profiles with suggested molecular arrangement of $F_{15}C_{18}$-PA (purple) compared with C_{18}-PA (black) and BTBT−C_{12}-PA (green) SAM. The electron density profiles indicate a tilted alkyl spacer chain and a surface-normal headgroup of the $F_{15}C_{18}$-PA SAM, and a surface-normal spacer chain and a tilted headgroup of the molecules in the BTBT−C_{12}-PA SAM.

poor part of the SAM with the anchor group was identified as 12.0 Å. The theoretical length of this part of the molecule is not reached, suggesting a tilt of the nonfunctionalized alkyl section of ∼47° relative to the surface normal (Figure 3b). The lower electron density compared with alkyl-PAs (0.32 e/Å^3) is a result of the spatial requirements of the fluorinated headgroup of the molecule, leading to a less dense packing of the alkyl region of the SAM. The fluorinated region is clearly resolved in the electron density profile by a distinct peak with an electron density of 0.78 e/Å^3 and a thickness of 10.0 Å, which is slightly larger than the theoretical length of the fluorinated component of the molecule (9.0 Å). This indicates an orientation of the functionalized segment perpendicular to the surface.

3.3. P-type Semiconductor Functionalized SAMs

The complexity and function of SAM molecules were further extended by implementing π-systems as functional head groups. These molecules serve as active layers in SAMFETs, where the semiconducting channel is realized solely by the 2D-arranged monolayer.[30−34] The device characteristics critically depend on the order and electrical interaction ($\pi\pi$-stacking) of the molecules. For these SAMs, XRR provides insight into the distribution and arrangement of the π-system, due to its higher electron density compared with the *n*-alkyl chain.

In this Account, a semiconducting monolayer from [12-(benzo[*b*]benzo[4,5]thieno[2,3-*d*]thiophen-2-yl)dodecyl)] phosphonic acid (BTBT−C_{12}-PA, Figure 1a) was self-assembled on an ALD grown AlO_x surface.[34] This molecule contains a semiconducting π-system (BTBT), which is connected to a C_{12} alkyl chain and a PA anchor group. A four-slab model was assumed for fitting the reflectivity data (Figure 3a), consisting of the AlO_x layer and the three building blocks of the molecule. The electron density profile of this system (Figure 3b, best fit parameters in Supporting Information, Table 1) reveals the conformation and packing of these molecules. The electron density drops from 0.89 e/Å^3 (AlO_x) to a 15 Å thick plateau with ρ_e of 0.24 e/Å^3, representing a surface-normal arrangement of the stretched C_{12} alkyl chain, followed by an electron-rich region of 0.48 e/Å^3 attributed to the BTBT headgroup. The surface-normal position of the π-system is confined to only 7.6 Å, indicating a tilted BTBT chromophore in the SAM. In addition to the driving force of the anchor group to bind on to the AlO_x surface, the $\pi\pi$-interaction of the BTBT head groups

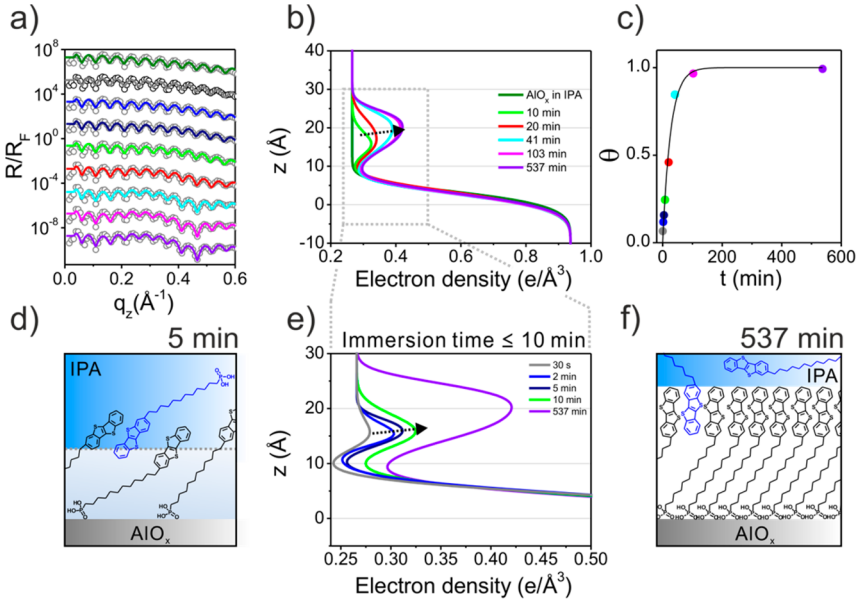

Figure 4. Investigation of the self-assembly process of a BTBT−C_{12}-PA SAM on AlO_x. (a) Measured R/R_F (circles) recorded before (substrate in IPA, green) and during the self-assembly of BTBT−C_{12}-PA molecules on AlO_x in IPA with corresponding fits (after 30 s, gray; 2 min, blue; 5 min, dark blue; 10 min, lime green; 20 min, red; 41 min, turquoise; 103 min, pink; 537 min, purple). Curves are shifted for clarity. (b) Evolution of the fit-derived electron density profiles of the BTBT−C_{12}-PA SAM over time. (c) Growth kinetics described by the coverage θ vs reaction time with experimental values and the corresponding fit, suggesting that the self-assembly follows a Langmuir isotherm type reaction path. (d) Schematic of the SAM condition at 5 min. (e) Electron density profiles of the beginning of SAM formation (≤10 min) compared with the profile of a fully assembled SAM (at 537 min, purple). (f) Schematic of the fully formed SAM at 537 min with single BTBT−C_{12}-PA molecules in solution and nonadsorbed molecules sticking in the SAM.

DOI: 10.1021/acs.accounts.5b00022
Acc. Chem. Res. 2015, 48, 1901−1908

contributes to the molecular arrangement within the homogeneous BTBT−C_{12}-PA system. We note that it is desirable to extend XRR measurements with GIXD experiments to also elaborate the lateral structure as an important feature that determines the efficiency of lateral charge transport in such SAMs on microscopic length scale.[22,31]

By performing in situ XRR during SAM formation of the BTBT−C_{12}-PA, further information on the early stages of self-assembly is obtained and how a confined chromophore packing is achieved is revealed.

3.3.1. In Situ XRR on a BTBT-C_{12}-PA System. In situ XRR has become a powerful tool for a detailed analysis of the formation of silane SAMs,[35] as well as thin organic[36] and inorganic films.[37] In this Account, the SAM formation of BTBT−C_{12}-PA on AlO_x was exemplarily studied in situ at the solid−liquid interface at beamline ID10 (ESRF, Grenoble). Subsequent to a reference scan, the first in situ scan was performed immediately after filling the coating cell with the SAM solution, followed by scans at selected immersion times.

SAM formation processes occur in a highly dynamic manner. In particular in the early stage,[15] the molecules can freely migrate at the substrate's surface. Hence, with the comparatively long reflectivity scan and admittedly small changes (Supporting Information, Figure 5) in the reflected signal, the electron density profiles have to be interpreted carefully. The corresponding best fit parameters (R/R_F in Figure 4a), assuming again a four-slab model, are tabulated in the Supporting Information. The evolution of the electron density profile is plotted in Figure 4b and displays a monotonic monolayer growth with the presence of a characteristic electron-rich region attributed to the BTBT headgroup. This becomes already visible during the first 10 min of self-assembly (Figure 4e). Immediately after deposition, a small depletion region at the AlO_x surface of lower electron-density (0.23 e/Å^3) compared with the electron density of the solvent is observed, which suggests a formation of a loosely packed layer by the first adsorbed molecules (Figure 4d) and a consequent reduction in the effective solvent density. As the packing density at the oxide surface increases, the depletion region in the profile disappears; at the same time, an increase in ρ_e occurs, which can be attributed to the BTBT headgroup. Both regions, the depletion layer, which becomes the region where the alkyl spacer of the molecule is predominantly located, and the BTBT chromophore layer, continuously increase in electron density and thickness over time. The initial ρ_e value of the depletion layer of 0.23 e/Å^3 (d = 7.3 Å) increases to a final electron density of 0.28 e/Å^3 (d = 10.6 Å) at 537 min, which is close to the expected density of alkanes in the rotator phase.[27] The electron density of the headgroup increases continuously from 0.30 e/Å^3 in the first in situ scan of the SAM and reaches a saturation value of 0.43 e/Å^3 (at 537 min), indicating a dense arrangement of the chromophores over time (Figure 4f). Small differences between the dried ex situ and the in situ electron density profiles can be explained by the environment of the deposited SAM. The alkyl backbone of the SAM appears to be tilted, while the increased length of the electron-rich region can be attributed to the BTBT chromophore arranged perpendicularly to the surface. Additionally, the $\pi\pi$-interaction between the BTBT cores of the nonadsorbed molecules (in solution) and the chromophores of the deposited SAM or a disordered multilayer build-up may lead to an increase in thickness of the electron-rich section.[30,38] Moreover, the kinetics of a BTBT SAM can be derived from such an in situ experiment. For this purpose, it is practical to define the coverage θ as the relative increase of the integrated electron density in the BTBT region with the electron densities of the BTBT headgroup (ρ_{BTBT}) and IPA (ρ_{IPA}), and thickness of the BTBT headgroup (d_{BTBT}):

$$\theta(t) = (\rho_{BTBT}(t) - \rho_{IPA})d_{BTBT}(t)$$

This coverage is displayed as a function of reaction time in Figure 4c, showing a drastic increase during the early stages, followed by a slow increase until a saturation level is reached, that is, the monolayer formation is completed. Commonly, such growth kinetics can be described by the Langmuir isotherm reaction,[39] which states that under the assumption that desorption is negligible

$$\theta = 1 - e^{(-k_a Ct)}$$

where C is the concentration and k_a is the adsorption rate constant.

The fit corresponding to this equation is depicted as the solid line in Figure 4c, showing good agreement with the experimental data, suggesting that the growth kinetics of a BTBT−C_{12}-PA SAM on AlO_x indeed follows a Langmuir isotherm type reaction path.

3.4. C_{60} Functionalized SAMs

In this section, we show a detailed analysis of the arrangement of more complex SAMs containing bulky head groups, such as fullerenes (Figure 1a). Generally, the monolayer assembly of C_{60} functionalized phosphonic acid molecules is dominated by the space requirements of the fullerene. The footprint of the anchor group and the cross section of the flexible linear alkyl chain normal to the long molecular axis are significantly smaller than the size of the attached fullerene in $C_{60}C_n$-PA molecules, which leads to a disordered SAM structure. SAMs of two C_{60} functionalized molecules (Figure 1a) were self-assembled on AlO_x: $C_{60}C_{18}$-PA with the fullerene attached to a flexible and long alkylphosphonic acid (C_{18}-PA) and $C_{60}C_6$-PA with a comparably short alkyl chain (C_6-PA).[20] Two-slab and four-slab electron density models were constructed for the $C_{60}C_6$-PA and the $C_{60}C_{18}$-PA SAM, respectively (R/R_F in Figure 5a; Supporting Information, Table 3, with best fit parameters). The corresponding electron density profiles of both SAMs (Figure 5b) exhibit high-ρ_e regions. In the case of $C_{60}C_6$-PA, this region is directly adjacent to the AlO_x surface (ρ_e = 0.56 e/Å^3, d = 21.7 Å) and is resolved without a drop in ρ_e, as seen in the case of $C_{60}C_{18}$-PA with a plateau of 11.6 Å and 0.36 e/Å^3.

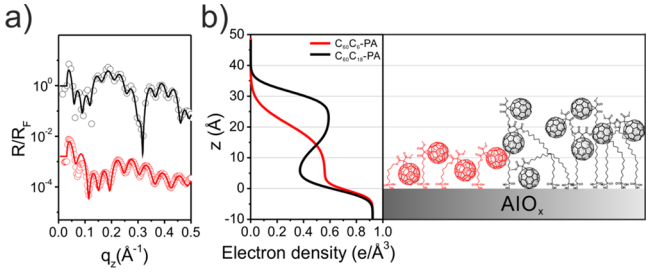

Figure 5. (a) Measured R/R_F (circles) and corresponding fits (solid lines) of a $C_{60}C_6$-PA[20] (red) and $C_{60}C_{18}$-PA[22] SAM (black) on AlO_x. Curves are shifted for clarity. (b) Fit-derived electron density profiles of a $C_{60}C_6$-PA SAM (red solid line) and $C_{60}C_{18}$-PA SAM (black solid line) with schematic interpretation. The profile of the $C_{60}C_{18}$-PA SAM exhibits an electron-poor section close to the substrate surface corresponding to the alkyl-dominated part of the SAM.

DOI: 10.1021/acs.accounts.5b00022
Acc. Chem. Res. 2015, 48, 1901−1908

This electron-poor section is attributed to the presence of flexible alkyl chains. The elevated electron density value compared with pure alkyl-PA SAMs (0.32 e/Å^3) suggests that a number of fullerenes are present in this region, but considerably less than further away from the substrate. Fullerenes possess a large number of electrons and thus, similar to the fluorinated alkyl-PA or BTBT−C_{12}-PA, a higher electron density compared with alkyl chains. However, due to the large diameter of the fullerene and the flexibility of alkyl chains, a confined layer of C_{60} at the top of the SAM is not obtained.[21] The thickness of the electron-rich region is significantly larger than the van-der-Waals diameter of C_{60} (roughly 10 Å).[40] In the case of $C_{60}C_{18}$-PA, it is 18.2 Å, displaying a broad distribution of fullerenes in the *z*-direction and suggesting a quasi-double layer of C_{60}.

4. MIXED C_{60} FUNCTIONALIZED SAMs

One possible approach to increase the order of molecules with bulky head groups (e.g., $C_{60}C_{18}$-PA) in SAMs is the incorporation of shorter supporting molecules such as alkylphosphonic acids.[21,22,41] This effect can be easily realized by mixing C_{60} functionalized molecules ($C_{60}C_{18}$-PA) with corresponding PAs, due to the same anchor group chemistry. The composition of the randomly mixed SAM on the surface is determined by the stoichiometry of the molecules in solution. We analyzed via XRR morphological variations upon changes in the stoichiometric composition of known mixed SAMs containing different electronic signatures.[21] Note that it is not possible from an XRR experiment to determine SAM components from unknown primary material or the stoichiometry of a known mixed SAM solution. However, it is possible to elucidate the differences in surface-normal morphology of mixed SAMs due to chain length variations of the supporting C_n-PA molecules. Mixed self-assembled monolayers (molar ratio of 1:1) of $C_{60}C_{18}$-PA in combination with C_{10}-PA, C_{14}-PA, C_{16}-PA, and C_{18}-PA (Figure 1a), as supporting components for the C_{60} headgroup, were deposited on AlO_x.[22] Their impact on the confinement of fullerene moieties in the *z*-direction across the substrate surface was investigated. A four-slab model (AlO_x, anchor group, alkyl chain, and C_{60} headgroup) was used for the modeling of measured reflectivity data (R/R_F in Figure 6a; best fit parameters in Supporting Information, Table 3). All fit-derived electron density profiles (Figure 6b) exhibit a similar shape with an electron-rich (mainly C_{60} head groups) and an electron-poor section (mainly alkyl chains and PA anchor), indicating the influence of alkyl-PA molecules on the confinement of C_{60} head groups. The electron density profile of a pure $C_{60}C_{18}$-PA SAM exhibits close to the AlO_x surface a slightly higher electron density of 0.36 e/Å^3 compared with 0.29−0.31 e/Å^3 for mixed systems. This is attributed to the presence of fullerenes (significantly higher electron density than alkyl-PA) due to a collapse of the flexible alkyl spacer. In mixed systems, this effect is prevented to a certain extent by the alkylphosphonic acid molecules, which fill the free space between the anchored $C_{60}C_{18}$-PA molecules and push C_{60}-moieties away from the substrate surface. This effect is displayed in the electron density profiles: within the parameter confidence intervals (Supporting Information, Table 3), the headgroup thickness shows a decreasing trend from pure $C_{60}C_{18}$-PA, over $C_{60}C_{18}$-PA/C_{10}-PA, $C_{60}C_{18}$-PA/C_{14}-PA, and $C_{60}C_{18}$-PA/C_{16}-PA, whereas for $C_{60}C_{18}$-PA/C_{18}-PA the relative thickness reduction is clearly significant. Here, the electron rich region (15.7 Å) is more confined and is located further away from the AlO_x surface. This seems reasonable due to the comparable length of the alkyl spacer in the functionalized $C_{60}C_{18}$-PA molecule. These XRR investigations support the picture of confined C_{60} head groups by supporting molecules and allow for discussing changes of in-depth morphology on the angstrom scale. This method was applied to improve the performance of SAMFET devices.[22]

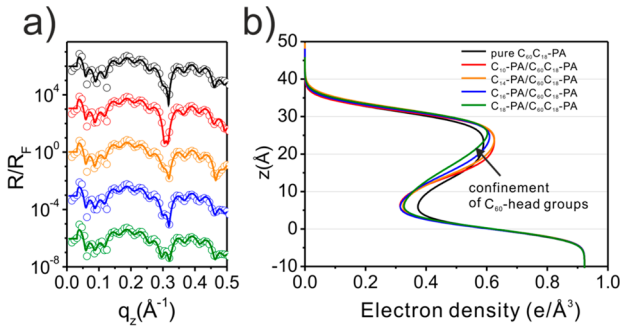

Figure 6. (a) Measured R/R_F (open circles) and corresponding fits[22] (solid lines) of pure $C_{60}C_{18}$-PA (black) and mixed C_n-PA/$C_{60}C_{18}$-PA SAMs with n = 10 (red), 14 (yellow), 16 (blue), and 18 (green) on AlO_x. Curves are shifted for clarity. (b) Fit-derived electron density profiles with a confinement of the C_{60} headgroup layer with increasing *n*-alkyl length.

5. CONCLUSIONS AND OUTLOOK

This Account summarizes recent results from the structural characterization of SAMs via XRR. Hereby, we obtained precise information on the layer thickness and surface-normal electron density distribution of the investigated SAMs. Further, conclusions on the molecular tilt angle and packing density were drawn. By investigation of various phosphonic acid derivatives on AlO_x surfaces, additional information on the driving forces of self-assembly were extracted. Functionalized molecules with a distinct distribution of electron density along the molecular chain exhibit a clear signature in the electron density profile and allow for conclusions about the molecular order. Additionally, XRR was efficiently utilized for the in situ tracking of the self-assembly process. Moreover, mixed SAMs from stoichometric solutions of $C_{60}C_{18}$-PA and alkyl-PA molecules have been applied on AlO_x. Their electron density profiles disclosed a trend of orientation of fullerenes with increasing supporting alkyl-PA length.

Our investigations delineate the way for a deeper understanding of film formation for applications such as organic electronics, where homogeneous layers are most beneficial and a distinct control of interface conditions is essential. Even though X-ray reflectivity represents a powerful tool to gather structural insight at the subnanometer scale of thin films, the use of complementary methods remains inevitable for a complete understanding of SAMs.

■ ASSOCIATED CONTENT

Supporting Information

Details on the XRR analysis, details on the in situ experiment, and tables with the fit-derived parameters for all systems. The Supporting Information is available free of charge on the ACS Publications website at DOI: 10.1021/acs.accounts.5b00022.

DOI: 10.1021/acs.accounts.5b00022
Acc. Chem. Res. 2015, 48, 1901−1908

AUTHOR INFORMATION

Author Contributions

A. K. and H.-G. S. contributed equally to this work.

Notes

The authors declare no competing financial interest.

Biographies

Artoem Khassanov received his diploma in Materials Science from Friedrich-Alexander-Universität Erlangen-Nürnberg in 2011, after undertaking a trainee program at the ESRF in Grenoble in 2010. Currently, he is a Ph.D. candidate studying self-assembled monolayers and their application in organic memory devices under supervision of Prof. Marcus Halik.

Hans-Georg Steinrück obtained his Ph.D. in Physics from the Friedrich-Alexander-Universität Erlangen-Nürnberg under the preceptorship of Prof. Andreas Magerl in 2015. He studies the self-assembly and surface-freezing of alkyl-derivatives on oxide surfaces.

Thomas Schmaltz obtained his Ph.D. in Materials Science at the Friedrich-Alexander-Universität Erlangen-Nürnberg under supervision of Prof. Marcus Halik in 2014. His work focuses on the self-assembly of functional organic molecules for application in organic electronics.

Andreas Magerl obtained his Ph.D. in 1979 from the Technische Universität München. After an engagement for some 20 years in international research facilities for neutron scattering, he joined the Friedrich-Alexander-Universität Erlangen-Nürnberg in 1997, where he is heading the Chair for Crystallography and Structural Physics.

Marcus Halik received his Ph.D. in Chemistry from the Martin-Luther Universität Halle-Wittenberg in 1998. After a postdoc at University of Arizona and five years in industry, he was appointed in 2005 to the Friedrich-Alexander-Universität Erlangen-Nürnberg, where he is head of the Organic Materials and Devices group. His research interests focus on organic electronics, molecular self-assembly and organic–inorganic hybrid materials.

ACKNOWLEDGMENTS

We acknowledge the German Research Council (DFG), the Collaborative Research Center 953, the Cluster of Excellence "Engineering of Advanced Materials – EXC 315" (www.eam.uni-erlangen.de), HA 2952/4–1, the DFG research unit 1878, "Functional Molecular Structures on Complex Oxide Surfaces", the Erlangen Graduate School of Molecular Science (GSMS), and the Interdisciplinary Center for Molecular Materials (ICMM). Further, we acknowledge the European Synchrotron Radiation Facility for provision of synchrotron radiation, and we thank Oleg Konovalov and Federico Zontone for assistance in using beamline ID10, as well as for fruitful, stimulating and helpful discussions.

REFERENCES

(1) Hotchkiss, P. J.; Jones, S. C.; Paniagua, S. A.; Sharma, A.; Kippelen, B.; Armstrong, N. R.; Marder, S. R. The Modification of Indium Tin Oxide with Phosphonic Acids: Mechanism of Binding, Tuning of Surface Properties, and Potential for Use in Organic Electronic Applications. *Acc. Chem. Res.* **2012**, *45*, 337–346.

(2) Queffélec, C.; Petit, M.; Janvier, P.; Knight, D. A.; Bujoli, B. Surface Modification Using Phosphonic Acids and Esters. *Chem. Rev.* **2012**, *112*, 3777–3807.

(3) Ma, H.; Acton, O.; Hutchins, D. O.; Cernetic, N.; Jen, A. K.-Y. Multifunctional Phosphonic Acid Self-Assembled Monolayers on Metal Oxides as Dielectrics, Interface Modification Layers and Semiconductors for Low-Voltage High-Performance Organic Field-Effect Transistors. *Phys. Chem. Chem. Phys.* **2012**, *14*, 14110–14126.

(4) Ulman, A. Formation and Structure of Self-Assembled Monolayers. *Chem. Rev.* **1996**, *96*, 1533–1554.

(5) Love, J. C.; Estroff, L. a; Kriebel, J. K.; Nuzzo, R. G.; Whitesides, G. M. Self-Assembled Monolayers of Thiolates on Metals as a Form of Nanotechnology. *Chem. Rev.* **2005**, *105*, 1103–1169.

(6) Pujari, S. P.; Scheres, L.; Marcelis, A. T. M.; Zuilhof, H. Covalent Surface Modification of Oxide Surfaces. *Angew. Chem., Int. Ed.* **2014**, *53*, 6322–6356.

(7) Schreiber, F. Structure and Growth of Self-Assembling Monolayers. *Prog. Surf. Sci.* **2000**, *65*, 151–257.

(8) Stöhr, J. *NEXAFS Spectroscopy*; Springer Series in Surface Sciences; Springer Berlin Heidelberg: Berlin, Heidelberg, 1992; Vol. *25*.

(9) Alt, M.; Schinke, J.; Hillebrandt, S.; Hänsel, M.; Hernandez-Sosa, G.; Mechau, N.; Glaser, T.; Mankel, E.; Hamburger, M.; Deing, K.; Jaegermann, W.; Pucci, A.; Kowalsky, W.; Lemmer, U.; Lovrincic, R. Processing Follows Function: Pushing the Formation of Self-Assembled Monolayers to High-Throughput Compatible Time Scales. *ACS Appl. Mater. Interfaces* **2014**, *6*, 20234–20241.

(10) Tillman, N.; Ulman, A.; Schildkraut, J. S.; Penner, T. L. Incorporation of Phenoxy Groups in Self-Assembled Monolayers of Trichlorosilane Derivatives. Effects on Film Thickness, Wettability, and Molecular Orientation. *J. Am. Chem. Soc.* **1988**, *110*, 6136–6144.

(11) Walter, S. R.; Youn, J.; Emery, J. D.; Kewalramani, S.; Hennek, J. W.; Bedzyk, M. J.; Facchetti, A.; Marks, T. J.; Geiger, F. M. In-Situ Probe of Gate Dielectric-Semiconductor Interfacial Order in Organic Transistors: Origin and Control of Large Performance Sensitivities. *J. Am. Chem. Soc.* **2012**, *134*, 11726–11733.

(12) Als-Nielsen, J.; Jacquemain, D.; Kjaer, K.; Leveiller, F.; Lahav, M.; Leiserowitz, L. Principles and Applications of Grazing Incidence X-Ray and Neutron Scattering from Ordered Molecular Monolayers at the Air-Water Interface. *Phys. Rep.* **1994**, *246*, 251–313.

(13) Thissen, P.; Valtiner, M.; Grundmeier, G. Stability of Phosphonic Acid Self-Assembled Monolayers on Amorphous and Single-Crystalline Aluminum Oxide Surfaces in Aqueous Solution. *Langmuir* **2010**, *26*, 156–164.

(14) Brodard-Severac, F.; Guerrero, G.; Maquet, J.; Florian, P.; Gervais, C.; Mutin, P. H. High-Field 17 O MAS NMR Investigation of Phosphonic Acid Monolayers on Titania. *Chem. Mater.* **2008**, *20*, 5191–5196.

(15) Lenz, T.; Schmaltz, T.; Novak, M.; Halik, M. Self-Assembled Monolayer Exchange Reactions as a Tool for Channel Interface Engineering in Low-Voltage Organic Thin-Film Transistors. *Langmuir* **2012**, *28*, 13900–13904.

(16) Zschieschang, U.; Yamamoto, T.; Takimiya, K.; Kuwabara, H.; Ikeda, M.; Sekitani, T.; Someya, T.; Klauk, H. Organic Electronics on Banknotes. *Adv. Mater.* **2011**, *23*, 654–658.

(17) Halik, M.; Klauk, H.; Zschieschang, U.; Schmid, G.; Dehm, C.; Schütz, M.; Maisch, S.; Effenberger, F.; Brunnbauer, M.; Stellacci, F. Low-Voltage Organic Transistors with an Amorphous Molecular Gate Dielectric. *Nature* **2004**, *431*, 963–966.

(18) Salinas, M.; Jäger, C. M.; Amin, A. Y.; Dral, P. O.; Meyer-Friedrichsen, T.; Hirsch, A.; Clark, T.; Halik, M. The Relationship between Threshold Voltage and Dipolar Character of Self-Assembled Monolayers in Organic Thin-Film Transistors. *J. Am. Chem. Soc.* **2012**, *134*, 12648–12652.

(19) Prado, M. C.; Neves, B. R. A. Mixed Self-Assembled Layers of Phosphonic Acids. *Langmuir* **2010**, *26*, 648–654.

(20) Khassanov, A.; Schmaltz, T.; Steinrück, H.-G.; Magerl, A.; Hirsch, A.; Halik, M. Interface Engineering of Molecular Charge Storage Dielectric Layers for Organic Thin-Film Memory Transistors. *Adv. Mater. Interfaces* **2014**, *1*, No. 1400238.

(21) Jäger, C. M.; Schmaltz, T.; Novak, M.; Khassanov, A.; Vorobiev, A.; Hennemann, M.; Krause, A.; Dietrich, H.; Zahn, D.; Hirsch, A.; Halik, M.; Clark, T. Improving the Charge Transport in Self-Assembled Monolayer Field-Effect Transistors: From Theory to Devices. *J. Am. Chem. Soc.* **2013**, *135*, 4893–4900.

DOI: 10.1021/acs.accounts.5b00022
Acc. Chem. Res. 2015, 48, 1901–1908

(22) Schmaltz, T.; Khassanov, A.; Steinrück, H.-G.; Magerl, A.; Hirsch, A.; Halik, M. Tuning the Molecular Order of C_{60}-Based Self-Assembled Monolayers in Field-Effect Transistors. *Nanoscale* **2014**, *6*, 13022−13027.
(23) Wang, Z.; Mohammadzadeh, S.; Schmaltz, T.; Kirschner, J.; Khassanov, A.; Eigler, S.; Mundloch, U.; Backes, C.; Steinrück, H.-G.; Magerl, A.; Hauke, F.; Hirsch, A.; Halik, M. Region-Selective Self-Assembly of Functionalized Carbon Allotropes from Solution. *ACS Nano* **2013**, *7*, 11427−11434.
(24) Pershan, P. S.; Schlossman, M. *Liquid Surfaces and Interfaces: Synchrotron X-Ray Methods*; Cambridge University Press: Cambridge, U.K., 2012.
(25) Nelson, A. Co-refinement of Multiple-Contrast Neutron/X-Ray Reflectivity Data Using MOTOFIT. *J. Appl. Crystallogr.* **2006**, *39*, 273−276.
(26) Smilgies, D. M.; Boudet, N.; Struth, B.; Konovalov, O. Troika II: A Versatile Beamline for the Study of Liquid and Solid Interfaces. *J. Synchrotron Radiat.* **2005**, *12*, 329−339.
(27) Ocko, B. M.; Wu, X. Z.; Sirota, E. B.; Sinha, S. K.; Gang, O.; Deutsch, M. Surface Freezing in Chain Molecules: Normal Alkanes. *Phys. Rev. E: Stat. Phys., Plasmas, Fluids, Relat. Interdiscip. Top.* **1997**, *55*, 3164−3182.
(28) Wasserman, S. R.; Whitesides, G. M.; Tidswell, I. M.; Ocko, B. M.; Pershan, P. S.; Axe, J. D. The Structure of Self-Assembled Monolayers of Alkylsiloxanes on Silicon: A Comparison of Results from Ellipsometry and Low-Angle X-Ray Reflectivity. *J. Am. Chem. Soc.* **1989**, *111*, 5852−5861.
(29) Novak, M.; Jäger, C. M.; Rumpel, A.; Kropp, H.; Peukert, W.; Clark, T.; Halik, M. The Morphology of Integrated Self-Assembled Monolayers and Their Impact on Devices − A Computational and Experimental Approach. *Org. Electron.* **2010**, *11*, 1476−1482.
(30) Smits, E. C. P.; Mathijssen, S. G. J.; van Hal, P. A.; Setayesh, S.; Geuns, T. C. T.; Mutsaers, K. A. H. A.; Cantatore, E.; Wondergem, H. J.; Werzer, O.; Resel, R.; Kemerink, M.; Kirchmeyer, S.; Muzafarov, A. M.; Ponomarenko, S. A.; de Boer, B.; Blom, P. W. M.; de Leeuw, D. M. Bottom-up Organic Integrated Circuits - Supplementary. *Nature* **2008**, *455*, 956−959.
(31) Mathijssen, S. G. J.; Smits, E. C. P.; van Hal, P. A.; Wondergem, H. J.; Ponomarenko, S. A.; Moser, A.; Resel, R.; Bobbert, P. A.; Kemerink, M.; Janssen, R. A. J.; de Leeuw, D. M. Monolayer Coverage and Channel Length Set the Mobility in Self-Assembled Monolayer Field-Effect Transistors. - Supplementary. *Nat. Nanotechnol.* **2009**, *4*, 674−680.
(32) Novak, M.; Ebel, A.; Meyer-Friedrichsen, T.; Jedaa, A.; Vieweg, B. F.; Yang, G.; Voitchovsky, K.; Stellacci, F.; Spiecker, E.; Hirsch, A.; Halik, M. Low-Voltage P- and N-Type Organic Self-Assembled Monolayer Field Effect Transistors. *Nano Lett.* **2011**, *11*, 156−159.
(33) Hutchins, D. O.; Acton, O.; Weidner, T.; Cernetic, N.; Baio, J. E.; Ting, G.; Castner, D. G.; Ma, H.; Jen, A. K.-Y. Spin Cast Self-Assembled Monolayer Field Effect Transistors. *Org. Electron.* **2012**, *13*, 464−468.
(34) Schmaltz, T.; Amin, A. Y.; Khassanov, A.; Meyer-Friedrichsen, T.; Steinrück, H.-G.; Magerl, A.; Segura, J. J.; Voitchovsky, K.; Stellacci, F.; Halik, M. Low-Voltage Self-Assembled Monolayer Field-Effect Transistors on Flexible Substrates. *Adv. Mater.* **2013**, *25*, 4511−4514.
(35) Richter, A. G.; Durbin, M. K.; Yu, C.-J.; Dutta, P. In Situ Time-Resolved X-Ray Reflectivity Study of Self-Assembly from Solution. *Langmuir* **1998**, *14*, 5980−5983.
(36) Kowarik, S.; Gerlach, A.; Sellner, S.; Schreiber, F.; Cavalcanti, L.; Konovalov, O. Real-Time Observation of Structural and Orientational Transitions during Growth of Organic Thin Films. *Phys. Rev. Lett.* **2006**, *96*, No. 125504.
(37) Ritley, K. A.; Just, K.; Schreiber, F.; Dosch, H.; Niesen, T. P.; Aldinger, F. X-Ray Reflectivity Study of Solution-Deposited ZrO_2 Thin Films on Self-Assembled Monolayers: Growth, Interface Properties, and Thermal Densification. *J. Mater. Res.* **2000**, *15*, 2706−2713.
(38) Hutchins, D. O.; Acton, O.; Weidner, T.; Cernetic, N.; Baio, J. E.; Castner, D. G.; Ma, H.; Jen, A. K.-Y. Solid-State Densification of Spun-Cast Self-Assembled Monolayers for Use in Ultra-Thin Hybrid Dielectrics. *Appl. Surf. Sci.* **2012**, *261*, 908−915.
(39) Wedler, G.; Freund, H.-J. *Lehrbuch Der Physikalischen Chemie*; Wiley VCH: Weinheim, Germany, 2012; Vol. 3.
(40) Krätschmer, W.; Lamb, L. D.; Fostiropoulos, K.; Huffman, D. R. Solid C_{60}: A New Form of Carbon. *Nature* **1990**, *347*, 354−358.
(41) Rumpel, A.; Novak, M.; Walter, J.; Braunschweig, B.; Halik, M.; Peukert, W. Tuning the Molecular Order of C_{60} Functionalized Phosphonic Acid Monolayers. *Langmuir* **2011**, *27*, 15016−15023.

DOI: 10.1021/acs.accounts.5b00022
Acc. Chem. Res. 2015, 48, 1901−1908